

Quantum Fisher Information Revealing Parameter Sensitivity in Long-Baseline Neutrino Experiments

Bhavna Yadav,* Amir Subba,† and Yu Shi‡

Wilczek Quantum Center, Shanghai Institute for Advanced Studies, Shanghai 201315, China
 University of Science and Technology of China, Hefei 230026, China

(Dated: February 6, 2026)

Determination of the leptonic CP-violating phase δ_{CP} , the atmospheric mixing angle θ_{23} , and the mass-squared difference Δm_{31}^2 constitutes a primary objective of current and next-generation long-baseline neutrino experiments. We employ QFI (QFI) to establish fundamental precision bounds on single-parameter estimation in three-flavor $\nu_\mu \rightarrow \nu_e$ oscillations, treating the neutrino as an evolving pure quantum state. Computing QFI as a function of the baseline-to-energy ratio L/E for benchmark parameter sets from NuFit-6.0, we find distinct sensitivity hierarchies and L/E -dependent structures. Specifically, δ_{CP} and θ_{23} exhibit bimodal QFI profiles with peaks at $L/E \sim 500$ and 1500 km/GeV, corresponding to the first and second oscillation maxima, reaching $F_Q(\delta_{CP}) \sim 0.15$ and $F_Q(\theta_{23}) \sim 15$, respectively. In contrast, Δm_{31}^2 displays a unimodal structure peaking at $L/E \sim 1000\text{--}1200$ km/GeV with $F_Q(\Delta m_{31}^2) \sim 3 \times 10^6$, reflecting its role in setting the oscillation length scale.

The discovery of neutrino oscillation has firmly established that neutrinos possess non-zero masses and undergo flavor transitions as they propagate, implying mixing among flavor and mass eigenstates [1–4]. This phenomenon is described by the Pontecorvo-Maki-Nakagawa-Sakata (PMNS) matrix, which is parameterized by three mixing angles, two independent mass-squared differences, and a CP-violating phase δ_{CP} [5, 6]. Precise determination of these oscillation parameters remains one of the central goals of neutrino physics [7–10]. In particular, the leptonic CP-violating phase δ_{CP} , the atmospheric mixing angle θ_{23} , and the atmospheric mass-squared difference Δm_{31}^2 play a crucial role in shaping oscillation probabilities at long-baseline experiments.

Among these, the measurement of δ_{CP} is of profound importance, as leptonic CP violation may provide key insights into the observed baryon asymmetry of the Universe through mechanisms such as Leptogenesis. At the same time, precise knowledge of θ_{23} is essential for resolving the octant ambiguity and understanding the structure of lepton mixing. Also the precise determination of Δm_{31}^2 is critical for establishing the neutrino mass ordering and for precision oscillation phenomenology. Current and forthcoming long-baseline neutrino experiments, including T2K [11], NO ν A [12], Hyper-Kamiokande [13], DUNE [14, 15], and ESS ν SB [16, 17], are expected to significantly improve sensitivity to these parameters. However, challenges such as parameter degeneracies, matter effects, statistical limitations, and systematic uncertainties continue to hinder their precise extraction.

In parallel with developments in neutrino phenomenology, concepts and tools from quantum information theory have increasingly been employed to understand and characterize neutrino oscillation dynamics [18–48]. Treating

oscillating neutrinos as evolving quantum states provides a natural framework to investigate their coherence, entanglement properties, and information-theoretic characteristics. Within this approach, QFI has emerged as a powerful quantity to quantify the ultimate precision limit with which a parameter can be estimated, as dictated by the quantum Cramér Rao bound [49]. Unlike classical estimators that depend on specific measurement strategies, QFI provides a measurement-independent bound and thus captures the fundamental information about a parameter encoded in a quantum state. It was also used in analyzing collider experiments [50].

Applying QFI to neutrino oscillations offers a rigorous and unified method to quantify the intrinsic sensitivity of the system to fundamental oscillation parameters [51, 52]. Evaluating QFI with respect to δ_{CP} , θ_{23} , and Δm_{31}^2 allows one to identify optimal conditions such as baseline length, neutrino energy, and experimental environment under which the precision on each parameter can be maximized. Moreover, QFI naturally incorporates the effects of matter interactions, correlations among oscillation parameters, and potential new physics scenarios, providing a model-independent quantum-information-based perspective on neutrino precision studies.

In this work, we investigate the role of QFI in the estimation of the three parameters δ_{CP} , θ_{23} , and Δm_{31}^2 , treating one parameter at a time within the three-flavor neutrino oscillation framework. By analyzing the evolution of neutrino states in vacuum, we examine how QFI encodes sensitivity to each parameter and study its dependence on key oscillation and experimental variables. Our analysis aims to identify parameter regimes where QFI is maximal and thereby establish fundamental precision limits on neutrino oscillation parameters, offering valuable guidance for current and future long-baseline neutrino experiments. As such, this work strengthens the connection between quantum information theory and neutrino physics, and provides deeper conceptual insights

* bhavnayadav04@ustc.edu.cn

† amirsubba@ustc.edu.cn

‡ yu.shi@ustc.edu.cn

into the quantum nature of neutrino oscillations.

Neutrino oscillation is a quantum mechanical phenomenon arising from the mismatch between neutrino flavor eigenstates and mass eigenstates [53, 54]. Neutrinos are produced and detected in flavor eigenstates $|\nu_\alpha\rangle$ ($\alpha = e, \mu, \tau$), which are linear superpositions of the mass eigenstates $|\nu_i\rangle$ ($i = 1, 2, 3$) with definite masses m_i . This mixing is described in terms of the unitary PMNS matrix U , such that $|\nu_\alpha\rangle = \sum_{i=1}^3 U_{\alpha i} |\nu_i\rangle$. As neutrinos propagate, mass eigenstates accumulate different quantum phases due to their distinct masses. For ultra-relativistic neutrinos with energy E , the time evolution of the i -th mass eigenstate is $|\nu_i(t)\rangle = e^{-i(E_i t - p_i L)} |\nu_i\rangle \approx \exp\left(-i\frac{m_i^2 L}{2E}\right) |\nu_i\rangle$, where $L \approx t$ in natural units. Consequently, the flavor composition evolves non-trivially with distance, leading to oscillations among flavors.

The probability of a neutrino produced as flavor ν_α being detected as flavor ν_β after traveling a distance L in vacuum is [53, 55] $P_{\alpha \rightarrow \beta} = \delta_{\alpha\beta} - 4 \sum_{i>j} \text{Re} \left(U_{\alpha i} U_{\beta i}^* U_{\alpha j}^* U_{\beta j} \right) \sin^2 \left(\frac{\Delta m_{ij}^2 L}{4E} \right) + 2 \sum_{i>j} \text{Im} \left(U_{\alpha i} U_{\beta i}^* U_{\alpha j}^* U_{\beta j} \right) \sin \left(\frac{\Delta m_{ij}^2 L}{2E} \right)$, where $\Delta m_{ij}^2 = m_i^2 - m_j^2$. The real term governs the oscillatory modulation, whereas the imaginary (CP-odd) term encodes leptonic CP violation through δ_{CP} . Thus, oscillations are sensitive to fundamental neutrino parameters: mixing angles θ_{ij} , mass-squared differences Δm_{21}^2 and $|\Delta m_{31}^2|$, and the CP-violating phase.

In realistic long-baseline and atmospheric neutrino experiments, neutrinos propagate through matter, where forward scattering with electrons modifies their effective Hamiltonian known as Mikheyev-Smirnov-Wolfenstein (MSW) [56, 57] effect. The MSW effect introduces an additional potential for electron neutrinos, altering effective mixing parameters and mass splittings. As a result, oscillation probabilities in matter can be significantly enhanced or suppressed depending on energy, baseline, and the neutrino mass ordering (normal or inverted). Matter effects can mimic or obscure CP-violating signals, making their proper inclusion essential for precise determination of δ_{CP} .

The neutrino oscillations thus represent a rich interferometric phenomenon arising from quantum coherence and phase accumulation, directly linking experimental observations to fundamental parameters of the lepton sector. Precise measurement of these parameters particularly the leptonic CP phase constitutes a primary objective of current and future long-baseline experiments such as T2K, NO ν A, Hyper-Kamiokande, and DUNE. Within this framework, studying neutrino oscillations using quantum information concepts, such as QFI, provides deeper insight into how efficiently oscillating neutrino states encode these parameters and what fundamental precision limits can be achieved.

QFI plays a central role in quantum parameter estimation theory, providing a fundamental bound on the precision with which an unknown parameter encoded in

a quantum state can be estimated. For a family of density matrices $\rho(\lambda)$ depending on a parameter λ , the ultimate lower bound on the variance of any unbiased estimator $\hat{\lambda}$ is dictated by the quantum Cramér-Rao bound [49]

$$(\Delta\lambda)^2 \geq \frac{1}{M F_Q(\lambda)}, \quad (1)$$

where M is the number of independent measurements and $F_Q(\lambda)$ is the QFI on parameter λ . Unlike classical Fisher Information (CFI), which depends on a particular measurement strategy and detection probability distribution, QFI is a property of the quantum state itself and therefore sets an absolute theoretical precision limit achievable by any optimal measurement.

QFI can be defined through the Symmetric Logarithmic Derivative (SLD) operator L_λ , which satisfies [58–61]

$$\frac{\partial \rho(\lambda)}{\partial \lambda} = \frac{1}{2} (\rho(\lambda) L_\lambda + L_\lambda \rho(\lambda)). \quad (2)$$

Then the QFI is given by [51]

$$F_Q(\lambda) = \text{Tr} [\rho(\lambda) L_\lambda^2]. \quad (3)$$

For pure states, $\rho(\lambda) = |\psi(\lambda)\rangle\langle\psi(\lambda)|$, the QFI (QFI) reduces to [58, 59, 62, 63] $F_Q(\lambda) = 4 [\langle\partial_\lambda \psi|\partial_\lambda \psi\rangle - |\langle\psi|\partial_\lambda \psi\rangle|^2]$. This expression makes explicit that the QFI quantifies the sensitivity of the quantum state to variations in the parameter λ . In the present analysis, we set $\lambda \in \{\delta_{\text{CP}}, \theta_{23}, \Delta m_{31}^2\}$. A more rapid change of the state with respect to a given parameter leads to a larger QFI and, consequently, a higher achievable precision in its estimation.

For a general mixed state expressed in its spectral decomposition

$$\rho(\lambda) = \sum_i p_i(\lambda) |i(\lambda)\rangle\langle i(\lambda)|, \quad (4)$$

the QFI has the form

$$F_Q(\lambda) = \sum_i \frac{(\partial_\lambda p_i)^2}{p_i} + 2 \sum_{i \neq j} \frac{(p_i - p_j)^2}{p_i + p_j} |\langle i|\partial_\lambda j\rangle|^2. \quad (5)$$

Once a specific measurement strategy is adopted, such as flavor detection at a far detector, the transition probabilities $P_{\alpha \rightarrow \beta}(\lambda)$ define the classical Fisher information,

$$F_C(\lambda) = \sum_\beta \frac{1}{P_{\alpha \rightarrow \beta}} \left(\frac{\partial P_{\alpha \rightarrow \beta}}{\partial \lambda} \right)^2. \quad (6)$$

A fundamental inequality holds,

$$F_C(\lambda) \leq F_Q(\lambda), \quad (7)$$

demonstrating that QFI represents the ultimate theoretical sensitivity limit, while the CFI quantifies what can be achieved by a given experimental configuration. When

Parameter	Normal Ordering (NO)		Inverted Ordering (IO)	
	Best fit $\pm 1\sigma$			
	(IC19 without SK-atm)	(IC24 with SK-atm)	(IC19 without SK-atm)	(IC24 with SK-atm)
θ_{12} [°]	$33.68^{+0.73}_{-0.70}$	$33.68^{+0.73}_{-0.70}$	$33.68^{+0.73}_{-0.70}$	$33.68^{+0.73}_{-0.70}$
θ_{23} [°]	$48.5^{+0.7}_{-0.9}$	$43.3^{+1.0}_{-0.8}$	$48.6^{+0.7}_{-0.9}$	$47.9^{+0.7}_{-0.9}$
θ_{13} [°]	$8.52^{+0.11}_{-0.11}$	$8.56^{+0.11}_{-0.11}$	$8.58^{+0.11}_{-0.11}$	$8.59^{+0.11}_{-0.11}$
δ_{CP} [°]	177^{+19}_{-20}	212^{+26}_{-41}	285^{+25}_{-28}	274^{+25}_{-23}
Δm_{21}^2 [10 $^{-5}$ eV 2]	$7.49^{+0.19}_{-0.19}$	$7.49^{+0.19}_{-0.19}$	$7.49^{+0.19}_{-0.19}$	$7.49^{+0.19}_{-0.19}$
Δm_{31}^2 [10 $^{-3}$ eV 2]	$+2.534^{+0.025}_{-0.023}$	$+2.513^{+0.021}_{-0.019}$	$-2.510^{+0.024}_{-0.025}$	$-2.484^{+0.020}_{-0.020}$

TABLE I. Best-fit values and 1σ ranges of the three-flavor neutrino oscillation parameters from NuFit-6.0 global analysis for the two datasets considered in this work [7].

an optimal measurement saturates this bound, the estimation precision reaches the quantum limit.

We now present numerical evaluations of the QFI for the individual estimation of the oscillation parameters δ_{CP} , θ_{23} , and Δm_{31}^2 . For each parameter, we vary it around its benchmark value while keeping the remaining parameters fixed, thereby isolating the intrinsic sensitivity of the neutrino state to a single parameter at a time. The results are expressed as functions of the baseline-to-energy ratio L/E , which captures the essential oscillation dynamics and allows for a transparent comparison of sensitivity across different experimental configurations.

Alongside QFI we focus on the $\nu_\mu \rightarrow \nu_e$ appearance probability in our analysis, as this channel provides the dominant sensitivity to the leptonic CP-violating phase δ_{CP} in long-baseline accelerator experiments. Unlike disappearance channels, $P_{\mu e}$ depends explicitly on δ_{CP} and is strongly affected by matter effects, enabling simultaneous sensitivity to the CP phase, the atmospheric mixing angle θ_{23} , and the neutrino mass ordering. Moreover, the appearance channel constitutes the primary measurement channel for current and future long-baseline experiments. Displaying $P_{\mu e}$ alongside the QFI therefore allows for a direct and physically transparent comparison between regions of enhanced quantum sensitivity and experimentally relevant oscillation maxima.

Throughout our analysis, we adopt benchmark values of the neutrino oscillation parameters consistent with the latest global-fit results. Unless stated otherwise, the mixing angles and mass-squared differences are fixed to the values listed in Table I. These benchmarks ensure consistency with previous studies and provide a standard reference for interpreting the QFI results.

In order to facilitate a direct connection between the QFI-based sensitivity analysis and realistic experimental configurations, we explicitly highlight the characteristic baseline to energy ratios corresponding to several accelerator-based long-baseline neutrino experiments. Specifically, we indicate the values of L/E associated with DUNE, NO ν A, T2K, MINOS, and ESS ν SB, where L denotes the experimental baseline and E corresponds to the neutrino energy at which the flux is maxi-

mal for each facility (see Appendix A for details on each experiments).

Figure 1 shows the QFI for δ_{CP} evaluated at two benchmark sets of oscillation parameters: NuFit IC24 including S-K atmospheric data (solid lines) and IC19 without atmospheric data (dashed lines), plotted as a function of L/E . The QFI exhibits two prominent peaks at $L/E \sim 500$ km/GeV and $L/E \sim 1500$ km/GeV, corresponding closely to the oscillation maxima in the transition probability $P(\nu_\mu \rightarrow \nu_e)$. No significant difference is observed between the two datasets, indicating that the intrinsic sensitivity to δ_{CP} is largely independent of these variations in experimental input. The observed behavior of the QFI is similar to that reported in Ref. [52], indicating consistency with previous studies of CP-phase sensitivity.

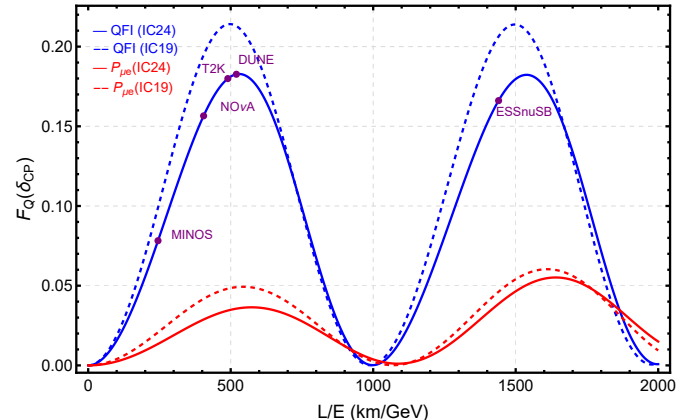


FIG. 1. QFI $F_Q(\delta_{CP})$ and the oscillation probability $P(\nu_\mu \rightarrow \nu_e)$ as functions of L/E . The blue curves show the QFI, while the red curves represent the transition probability. Solid lines correspond to the NuFit-6.0 IC24 dataset including Super-Kamiokande (S-K) atmospheric data, whereas dashed lines correspond to the IC19 dataset without S-K data.

The atmospheric mixing angle θ_{23} exhibits a qualitatively similar QFI behavior to δ_{CP} , with a bimodal structure featuring peaks at $L/E \sim 500$ km/GeV and

$L/E \sim 1500$ km/GeV, as shown in Fig. 2. These peaks correspond to the first and second oscillation maxima where matter effects in $P(\nu_\mu \rightarrow \nu_e)$ are most pronounced. However, θ_{23} demonstrates significantly enhanced quantum sensitivity, with peak values reaching $F_Q(\theta_{23}) \sim 15$ approximately two orders of magnitude larger than $F_Q(\delta_{CP}) \sim 0.15$. Via the quantum Cramér-Rao bound in Eq. (1), this translates to substantially tighter theoretical precision limits for the atmospheric mixing angle. The negligible separation between IC24 (solid) and IC19 (dashed) curves indicates that the quantum information content for θ_{23} is insensitive to the inclusion of Super-Kamiokande atmospheric data in global fits. Experiments operating near the first oscillation maximum (DUNE, T2K and NO ν A) achieve peak sensitivity at $L/E \sim 500$ km/GeV, while ESS ν SB, designed for the second maximum, attains comparable peak QFI at $L/E \sim 1500$ km/GeV, demonstrating the complementary sensitivity of different baseline configurations.

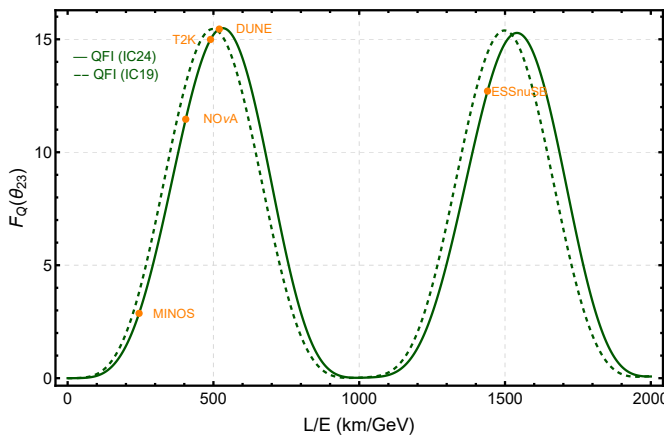


FIG. 2. QFI for Θ_{23} as functions of L/E . The green curves show QFI where solid line correspond to the NuFit-6.0 IC24 dataset including S-K atmospheric data, whereas dashed line correspond to the IC19 dataset without S-K data.

The mass-squared difference Δm_{31}^2 exhibits a markedly different QFI behavior compared to the angular parameters, as shown in Fig. 3. In contrast to the bimodal structure observed for δ_{CP} and θ_{23} , which closely track the oscillation maxima in $P(\nu_\mu \rightarrow \nu_e)$, the QFI for Δm_{31}^2 exhibits a single broad maximum centered at $L/E \sim 1000$ – 1200 km/GeV, with peak values reaching $F_Q(\Delta m_{31}^2) \sim 3 \times 10^6$. This represents an enhancement of nearly five orders of magnitude relative to δ_{CP} and over four orders of magnitude compared to θ_{23} . The unimodal profile arises from the distinct role of Δm_{31}^2 in the oscillation dynamics: whereas angular parameters modulate amplitudes and phases at specific oscillation maxima, the mass-squared difference sets the oscillation length $\lambda_{osc} \propto E/\Delta m^2$, leading to cumulative sensitivity across a broader L/E range. The quantum bound indicates exceptionally stringent theoretical precision limits for mass-squared difference determination. Notably, the QFI peak

does not coincide with the baseline-to-energy ratios of any single experimental configuration, but rather reflects an optimal intermediate regime for Δm_{31}^2 measurement. The minimal discrepancy between IC24 (solid) and IC19 (dashed) curves confirms the robustness of quantum information extraction for Δm_{31}^2 across different global fit scenarios.

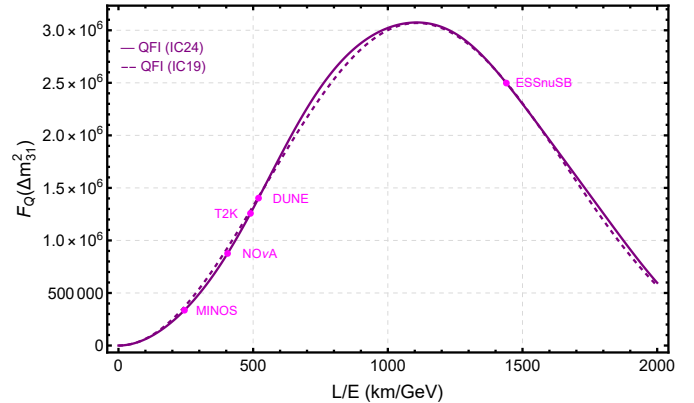


FIG. 3. QFI for Δm_{31}^2 as function of L/E . The purple curves show QFI, where solid line correspond to the NuFit-6.0 IC24 dataset including S-K atmospheric data, whereas dashed line correspond to the IC19 dataset without S-K data.

This study extends previous quantum estimation analyses of δ_{CP} [52] to include θ_{23} and Δm_{31}^2 , demonstrating that QFI provides a unified, theory-driven framework to identify optimal experimental configurations and establish fundamental precision benchmarks. The framework is particularly valuable for guiding the design of next-generation facilities, as it isolates intrinsic quantum limits from experimental systematics. Future work could extend this analysis to multi-parameter estimation, where quantum correlations between parameters may modify optimal measurement strategies.

To summarize, We have investigated QFI as a fundamental measure of parameter sensitivity in three-flavor neutrino oscillations, providing a measurement-independent assessment of the ultimate precision limits imposed by quantum mechanics. Focusing on single-parameter estimation in the $\nu_\mu \rightarrow \nu_e$ appearance channel, we computed the QFI for the CP-violating phase δ_{CP} , the atmospheric mixing angle θ_{23} , and the mass-squared difference Δm_{31}^2 as functions of the ratio L/E , evaluated at two benchmark parameter sets from NuFit-6.0 (IC24 with Super-Kamiokande atmospheric data and IC19 without).

Our analysis reveals a pronounced hierarchy in quantum sensitivity: $F_Q(\Delta m_{31}^2) \sim 3 \times 10^6$ exceeds $F_Q(\theta_{23}) \sim 15$ by over four orders of magnitude, which in turn surpasses $F_Q(\delta_{CP}) \sim 0.15$ by two orders of magnitude. Through the quantum Cramér-Rao bound $\Delta\theta \geq 1/\sqrt{F_Q(\theta)}$, these disparities translate directly into the attainable precision for each parameter. The QFI for δ_{CP} and θ_{23} exhibit bimodal structures with peaks at

$L/E \sim 500$ km/GeV and $L/E \sim 1500$ km/GeV, coinciding with the first and second oscillation maxima in the transition probability $P(\nu_\mu \rightarrow \nu_e)$. These peaks align with the operational regimes of current and planned experiments: DUNE, T2K, and NO ν A operate near the first maximum, while ESS ν SB targets the second maximum. In contrast, Δm_{31}^2 displays a single broad maximum centered at $L/E \sim 1000$ –1200 km/GeV, reflecting its distinct role in controlling the oscillation length rather than modulating transition amplitudes at specific resonances. The minimal variation between IC24 and IC19 results confirms that quantum information extraction is robust against current uncertainties in global oscillation parameter fits.

This work was supported by National Natural Science Foundation (Grant Nos. T2241005 and 12075059).

Appendix A: Experimental Parameters for Long-Baseline Neutrino Facilities

The representative L/E values indicated in our results correspond to the characteristic kinematic regimes of accelerator-based long-baseline neutrino oscillation experiments. Table II summarizes the baseline length L , peak neutrino energy E_{peak} , and the resulting L/E ratio for each facility.

TABLE II. Baseline configurations and characteristic L/E values for long-baseline neutrino experiments.

Experiment	L (km)	E_{peak} (GeV)	L/E (km/GeV)
MINOS [64]	735	3.0	245
T2K [10, 11]	295	0.6	490
NO ν A [12]	810	2.0	405
DUNE [14, 15]	1300	2.5	520
ESS ν SB [16, 17]	360	0.25	1440

Appendix B: Comparison between Normal and Inverted Ordering

We also extend the single-parameter QFI analysis to compare the normal ordering (NO) and inverted ordering (IO) scenarios. The purpose of this comparison is to assess the dependence of the QFI on the neutrino mass ordering and to examine the robustness of the intrinsic quantum sensitivity against this discrete ambiguity. All results shown here correspond to the NuFit-6.0 IC24 benchmark dataset including S-K atmospheric data.

Figure 4 shows the QFI for the CP-violating phase δ_{CP} as a function of L/E for both NO and IO. The QFI peaks for NO and IO occur at identical L/E values, indicating no observable shift in peak positions. The peak magnitudes are comparable, with a mild enhancement of the

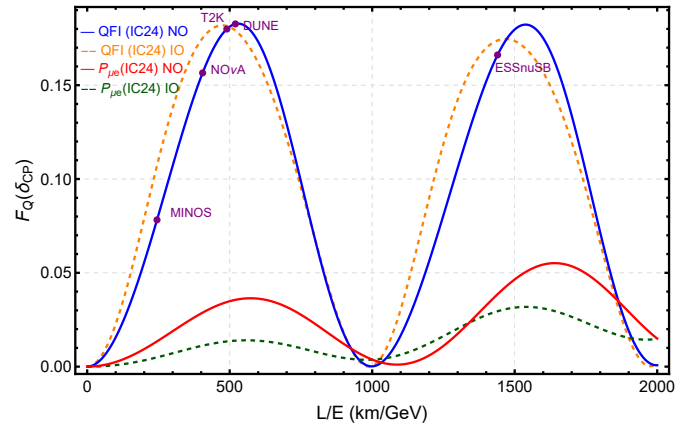


FIG. 4. QFI $F_Q(\delta_{\text{CP}})$ and the $\nu_\mu \rightarrow \nu_e$ oscillation probability as functions of L/E for the NuFit-6.0 IC24 dataset including S-K atmospheric data. The blue solid and orange dashed curves show the QFI for NO and IO, respectively. The red solid and green dashed curves represent the corresponding $\nu_\mu \rightarrow \nu_e$ transition probabilities for NO and IO.

second peak for IO at the level of a few percent, while the first peak remains unchanged.

T2K and DUNE lie close to the first QFI maximum for both ordering, indicating that these experiments operate near an optimal region for probing δ_{CP} . NO ν A is located in an intermediate L/E region between the first maximum and the rising part of the QFI curve, while MINOS lies at significantly lower L/E , where the QFI is comparatively small. ESS ν SB is positioned near the second oscillation maximum, which corresponds to an enhanced QFI region for normal ordering and remains close to the secondary peak for inverted ordering.

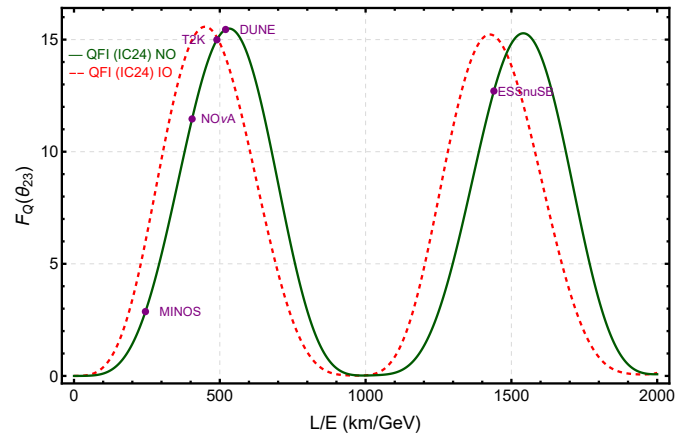


FIG. 5. QFI $F_Q(\Theta_{23})$ as function of L/E for the NuFit-6.0 IC24 dataset including S-K atmospheric data. The green solid and red dashed curves show the QFI for normal ordering (NO) and inverted ordering (IO), respectively.

For θ_{23} (see Fig. 5), the QFI peak heights are nearly identical for NO and IO, whereas both peaks exhibit a noticeable shift in their L/E positions, constituting the

dominant ordering-dependent effect for this parameter. A similar behavior to that for δ_{CP} is observed for the representative L/E values of long-baseline experiments, with T2K and DUNE near the first QFI maximum, ESS ν SB near the second maximum of IO, NO ν A in an intermediate region, and MINOS at lower L/E .

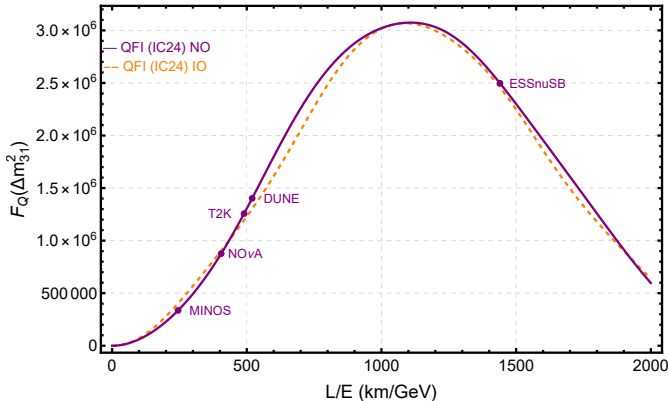


FIG. 6. Distribution of QFI for Δ_{23}^2 obtained against varying L/E for the NuFit-6.0 IC24 dataset including S-K atmospheric data. The purple solid and orange dashed curves show the QFI for normal ordering (NO) and inverted ordering (IO), respectively.

In contrast, for Δm_{31}^2 shown in Fig. 6, the QFI curves for NO and IO are essentially indistinguishable across the entire L/E range, with no observable differences in either peak positions or magnitudes. The representative L/E values of different experiments are indicated by dots in the figure. Among these, ESS ν SB lies closest to the region of maximal QFI, while DUNE, T2K, and NO ν A are located at somewhat lower L/E values and MINOS lies further away from the optimal region.

[1] Y. Fukuda *et al.* (Super-Kamiokande), Evidence for oscillation of atmospheric neutrinos, *Phys. Rev. Lett.* **81**, 1562 (1998), [arXiv:hep-ex/9807003](https://arxiv.org/abs/hep-ex/9807003).

[2] Q. R. Ahmad *et al.* (SNO), Direct evidence for neutrino flavor transformation from neutral current interactions in the Sudbury Neutrino Observatory, *Phys. Rev. Lett.* **89**, 011301 (2002), [arXiv:nucl-ex/0204008](https://arxiv.org/abs/nucl-ex/0204008).

[3] T. Araki *et al.* (KamLAND), Measurement of neutrino oscillation with KamLAND: Evidence of spectral distortion, *Phys. Rev. Lett.* **94**, 081801 (2005), [arXiv:hep-ex/0406035](https://arxiv.org/abs/hep-ex/0406035).

[4] K. Abe *et al.* (Super-Kamiokande), Solar Neutrino Measurements in Super-Kamiokande-IV, *Phys. Rev. D* **94**, 052010 (2016), [arXiv:1606.07538 \[hep-ex\]](https://arxiv.org/abs/1606.07538).

[5] Z. Maki, M. Nakagawa, and S. Sakata, Remarks on the unified model of elementary particles, *Progress of Theoretical Physics* **28**, 870 (1962), <https://academic.oup.com/ptp/article-pdf/28/5/870/5258750/28-5-870.pdf>.

[6] S. M. Bilenky and B. Pontecorvo, Lepton Mixing and Neutrino Oscillations, *Phys. Rept.* **41**, 225 (1978).

[7] I. Esteban, M. C. Gonzalez-Garcia, M. Maltoni, I. Martinez-Soler, J. P. Pinheiro, and T. Schwetz, NuFit-6.0: updated global analysis of three-flavor neutrino oscillations, *JHEP* **12**, 216, [arXiv:2410.05380 \[hep-ph\]](https://arxiv.org/abs/2410.05380).

[8] U. Rahaman, S. Razzaque, and S. U. Sankar, A Review of the Tension between the T2K and NO ν A Appearance Data and Hints to New Physics, *Universe* **8**, 109 (2022), [arXiv:2201.03250 \[hep-ph\]](https://arxiv.org/abs/2201.03250).

[9] F. Di Lodovico, R. B. Patterson, M. Shiozawa, and E. Worcester, Experimental Considerations in Long-baseline Neutrino Oscillation Experiments, *Baseline Neutrino Oscillation Measurements*, *Ann. Rev. Nucl. Part. Sci.* **73**, 69 (2023).

[10] S. Abubakar *et al.* (T2K, NO ν A), Joint neutrino oscillation analysis from the T2K and NO ν A experiments, *Nature* **646**, 818 (2025), [arXiv:2510.19888 \[hep-ex\]](https://arxiv.org/abs/2510.19888).

[11] J. Hu (Super-Kamiokande, T2K), Neutrino Oscillation Analysis with Combined Data from Super-Kamiokande and T2K, *PoS ICHEP2024*, 140 (2025).

[12] A. Kalitkina (NO ν A), NO ν A Recent Results of Three-Flavor Oscillation Analysis, *Phys. Atom. Nucl.* **88**, 443 (2025).

[13] C. Dalmazzone (Hyper-Kamiokande), Measurement of the CP violation in neutrino flavour oscillations with Hyper-Kamiokande, *PoS EPS-HEP2025*, 156 (2026).

[14] R. Acciari *et al.* (DUNE), Long-Baseline Neutrino Facility (LBNF) and Deep Underground Neutrino Experiment (DUNE): Conceptual Design Report, Volume 2: The Physics Program for DUNE at LBNF, (2015), [arXiv:1512.06148 \[physics.ins-det\]](https://arxiv.org/abs/1512.06148).

[15] L. Pérez-Molina (DUNE), DUNE Status and Science, *PoS EPS-HEP2025*, 180 (2026).

[16] A. Giannetti (ESSnuSB), ESSnuSB+ Project: Towards Precision Measurement of the CP Violation at the Second Neutrino Oscillation Maximum, *PoS EPS-HEP2023*, 155 (2024).

[17] M. Ghosh (ESSnuSB), Physics with next generation neutrino experiments: ESSnuSB, in *46th International Conference of Theoretical Physics Matter To The Deepest: Recent Developments In Physics Of Fundamental Interactions* (2026) [arXiv:2601.10271 \[hep-ph\]](https://arxiv.org/abs/2601.10271).

[18] M. Blasone, F. Dell'Anno, S. De Siena, M. Di Mauro, and

F. Illuminati, Multipartite entangled states in particle mixing, *Phys. Rev. D* **77**, 096002 (2008), arXiv:0711.2268 [quant-ph].

[19] M. Blasone, F. Dell'Anno, S. De Siena, and F. Illuminati, Entanglement in neutrino oscillations, *EPL* **85**, 50002 (2009), arXiv:0707.4476 [hep-ph].

[20] M. Blasone, F. Dell'Anno, S. De Siena, and F. Illuminati, Neutrino flavor entanglement, *Nucl. Phys. B Proc. Suppl.* **237-238**, 320 (2013).

[21] A. K. Alok, S. Banerjee, and S. U. Sankar, Quantum correlations in terms of neutrino oscillation probabilities, *Nucl. Phys. B* **909**, 65 (2016), arXiv:1411.5536 [hep-ph].

[22] M. Blasone, F. Dell'Anno, S. De Siena, and F. Illuminati, Flavor entanglement in neutrino oscillations in the wave packet description, *EPL* **112**, 20007 (2015), arXiv:1510.06761 [quant-ph].

[23] S. Banerjee, A. K. Alok, R. Srikanth, and B. C. Hiesmayr, A quantum information theoretic analysis of three flavor neutrino oscillations, *Eur. Phys. J. C* **75**, 487 (2015), arXiv:1508.03480 [hep-ph].

[24] J. A. Formaggio, D. I. Kaiser, M. M. Murskyj, and T. E. Weiss, Violation of the Leggett-Garg Inequality in Neutrino Oscillations, *Phys. Rev. Lett.* **117**, 050402 (2016), arXiv:1602.00041 [quant-ph].

[25] J. Naikoo, A. K. Alok, S. Banerjee, S. Uma Sankar, G. Guarneri, C. Schultze, and B. C. Hiesmayr, A quantum information theoretic quantity sensitive to the neutrino mass-hierarchy, *Nucl. Phys. B* **951**, 114872 (2020), arXiv:1710.05562 [hep-ph].

[26] Q. Fu and X. Chen, Testing violation of the Leggett-Garg-type inequality in neutrino oscillations of the Daya Bay experiment, *Eur. Phys. J. C* **77**, 775 (2017), arXiv:1705.08601 [hep-ph].

[27] M. Richter-Laskowska, M. Lobejko, and J. Dajka, Quantum contextuality of a single neutrino under interactions with matter, *New J. Phys.* **20**, 063040 (2018).

[28] J. Naikoo, A. Kumar Alok, S. Banerjee, and S. Uma Sankar, Leggett-Garg inequality in the context of three flavour neutrino oscillation, *Phys. Rev. D* **99**, 095001 (2019), arXiv:1901.10859 [hep-ph].

[29] D. Wang, F. Ming, X.-K. Song, L. Ye, and J.-L. Chen, Entropic uncertainty relation in neutrino oscillations, *Eur. Phys. J. C* **80**, 800 (2020).

[30] A. K. Jha, S. Mukherjee, and B. A. Bambah, Tri-Partite entanglement in Neutrino Oscillations, *Mod. Phys. Lett. A* **36**, 2150056 (2021), arXiv:2004.14853 [hep-ph].

[31] K. Dixit and A. K. Alok, New physics effects on quantum coherence in neutrino oscillations, *The European Physical Journal Plus* **136**, 10.1140/epjp/s13360-021-01311-4 (2021).

[32] T. Sarkar and K. Dixit, Effects of nonstandard interaction on temporal and spatial correlations in neutrino oscillations, *Eur. Phys. J. C* **81**, 88 (2021), arXiv:2010.02175 [hep-ph].

[33] S. Shafaq and P. Mehta, Enhanced violation of Leggett-Garg inequality in three flavour neutrino oscillations via non-standard interactions, *J. Phys. G* **48**, 085002 (2021), arXiv:2009.12328 [hep-ph].

[34] V. A. S. V. Bittencourt, M. Blasone, S. De Siena, and C. Matrella, Complete complementarity relations for quantum correlations in neutrino oscillations, *Eur. Phys. J. C* **82**, 566 (2022), arXiv:2205.01601 [quant-ph].

[35] B. Yadav, T. Sarkar, K. Dixit, and A. K. Alok, Can NSI affect non-local correlations in neutrino oscillations?, *Eur. Phys. J. C* **82**, 446 (2022), arXiv:2201.05580 [hep-ph].

[36] Y.-W. Li, L.-J. Li, X.-K. Song, D. Wang, and L. Ye, Genuine tripartite entanglement in three-flavor neutrino oscillations, *Eur. Phys. J. C* **82**, 799 (2022), arXiv:2205.11058 [quant-ph].

[37] Y.-W. Li, L.-J. Li, X.-K. Song, and D. Wang, Trade-off relations of quantum resource theory in neutrino oscillations, *Eur. Phys. J. Plus* **137**, 1267 (2022), arXiv:2212.09320 [quant-ph].

[38] A. K. Jha, A. Chatla, and B. A. Bambah, Neutrinos as qubits and qutrits, *Eur. Phys. J. Plus* **139**, 68 (2024), arXiv:2203.13485 [hep-ph].

[39] Z. A. Ravari, M. M. Ettefaghi, and S. Miraboutalebi, Quantum coherence in neutrino oscillation in matter, *Eur. Phys. J. Plus* **137**, 488 (2022), arXiv:2204.12332 [quant-ph].

[40] V. A. S. V. Bittencourt, M. Blasone, S. De Siena, and C. Matrella, Quantifying quantumness in three-flavor neutrino oscillations, *Eur. Phys. J. C* **84**, 301 (2024), arXiv:2305.06095 [quant-ph].

[41] G.-J. Wang, Y.-W. Li, L.-J. Li, X.-K. Song, and D. Wang, Monogamy properties of quantum correlations in neutrino oscillations, *Eur. Phys. J. C* **83**, 801 (2023).

[42] D. S. Chattpadhyay and A. Dighe, Quantum mismatch: A powerful measure of quantumness in neutrino oscillations, *Phys. Rev. D* **108**, 112013 (2023), arXiv:2304.02475 [hep-ph].

[43] K. Dixit, S. S. Haque, and S. Razzaque, Quantum spread complexity in neutrino oscillations, *Eur. Phys. J. C* **84**, 260 (2024), arXiv:2305.17025 [hep-ph].

[44] Soni, Bhavya and Shafaq, Sheeba and Mehta, Poonam, Distinguishing between Dirac and Majorana neutrinos using temporal correlations, (2023), arXiv:2307.04496 [hep-ph].

[45] L. Konwar and B. Yadav, NSI effects on tripartite entanglement in neutrino oscillations, *Nucl. Phys. B* **1002**, 116544 (2024), arXiv:2402.09952 [hep-ph].

[46] L. Konwar, J. Vardani, and B. Yadav, Violation of LGtI inequalities in the light of NO ν A and T2K anomaly, *Eur. Phys. J. C* **84**, 1103 (2024), arXiv:2401.02886 [hep-ph].

[47] B. Yadav and A. K. Alok, Impact of scalar NSI on spatial and temporal correlations in neutrino oscillations, *J. Phys. G* **52**, 125004 (2025), arXiv:2411.17503 [hep-ph].

[48] L. Konwar, P. Panda, and R. Mohanta, Effect of Off-diagonal NSI Parameters on Entanglement Measurements in Neutrino Oscillations, (2025), arXiv:2507.04885 [hep-ph].

[49] H. Cramér, *Mathematical Methods of Statistics* (Princeton University Press, Princeton, NJ, 1946) reprinted 1999, Princeton Landmarks in Mathematics and Physics.

[50] T. Ai, Q. Bi, Y. He, J. Liu, and X.-P. Wang, Ultimate quantum precision limit at colliders: Conditions and case studies, *Phys. Rev. Lett.* **135**, 241804 (2025).

[51] E. C. Nogueira, G. de Souza, A. D. Varizi, and M. D. Sampaio, Quantum estimation in neutrino oscillations, *Int. J. Quant. Inf.* **15**, 1750045 (2017), arXiv:1610.05388 [quant-ph].

[52] M. Ignoti, C. Frugueule, M. G. A. Paris, and M. G. Genoni, Is the large uncertainty of δ_{CP} fundamentally encoded in the neutrino quantum state?, (2025), arXiv:2511.20148 [hep-ph].

[53] C. Giunti and C. W. Kim, *Fundamentals of Neutrino Physics and Astrophysics* (2007).

[54] T. Ohlsson and H. Snellman, Three flavor neutrino oscillations in matter, *J. Math. Phys.* **41**, 2768 (2000), [Erratum: J.Math.Phys. 42, 2345 (2001)], arXiv:hep-ph/9910546.

[55] O. Yasuda, On the exact formula for neutrino oscillation probability by Kimura, Takamura and Yokomakura, (2007), arXiv:0704.1531 [hep-ph].

[56] L. Wolfenstein, Neutrino Oscillations in Matter, *Phys. Rev. D* **17**, 2369 (1978).

[57] S. P. Mikheyev and A. Y. Smirnov, Resonance Amplification of Oscillations in Matter and Spectroscopy of Solar Neutrinos, *Sov. J. Nucl. Phys.* **42**, 913 (1985).

[58] S. L. Braunstein and C. M. Caves, Statistical distance and the geometry of quantum states, *Phys. Rev. Lett.* **72**, 3439 (1994).

[59] M. G. A. Paris, Quantum Estimation for Quantum Technology, *Int. J. Quant. Inf.* **07**, 125 (2009), arXiv:0804.2981 [quant-ph].

[60] K. Jacobs, *Quantum Measurement Theory and its Applications* (Cambridge University Press, 2014).

[61] G. Tóth and I. Apellaniz, Quantum metrology from a quantum information science perspective, *J. Phys. A* **47**, 424006 (2014), arXiv:1405.4878 [quant-ph].

[62] C. W. Helstrom, *Quantum Detection and Estimation Theory* (Academic Press, 1976).

[63] L. Pezzè, A. Smerzi, M. K. Oberthaler, R. Schmied, and P. Treutlein, Quantum metrology with nonclassical states of atomic ensembles, *Rev. Mod. Phys.* **90**, 035005 (2018).

[64] P. Adamson *et al.* (MINOS), A Study of Muon Neutrino Disappearance Using the Fermilab Main Injector Neutrino Beam, *Phys. Rev. D* **77**, 072002 (2008), arXiv:0711.0769 [hep-ex].